Biomimetic artificial cells to model the effect of membrane asymmetry on chemoresistance

Elanna B. Stephenson & Katherine S. Elvira

2021

Journal Name

ARTICLE TYPE

Cite this: DOI: 00.0000/xxxxxxxxxx

Biomimetic artificial cells to model the effect of membrane asymmetry on chemoresistance†

Elanna B. Stephenson, and Katherine S. Elvira[a]

Received Date
Accepted Date

DOI: 00.0000/xxxxxxxxxx

We present a microfluidic platform that enables the formation of bespoke asymmetric droplet interface bilayers (DIBs) as artificial cell models from naturally-derived lipids. We use them to perform pharmacokinetic assays to quantify how lipid asymmetry affects the permeability of the chemotherapy drug doxorubicin. Previous attempts to model bilayer asymmetry with DIBs have relied on the use of synthetic lipids to achieve asymmetry. Use of natural lipids serves to increase the biomimetic nature of these artificial cells, showcasing the next step towards forming a true artificial cell membrane *in vitro*. Here we use our microfluidic platform to form biomimetic, asymmetric and symmetric DIBs, with their asymmetry quantified through their life-mimicking degree of curvature. We subsequently examine permeability of these membranes to doxorubicin, and reveal measurable differences in its pharmacokinetics induced by membrane asymmetry, highlighting another factor that potentially contributes to chemoresistance in some forms of cancer.

The lipid membrane of living cells contains several anatomical features which model membranes should replicate in order to be described as biomimetic. One of these is that the distribution of phospholipids is different between the inner and outer leaflets of eukaryotic cell bilayers. This asymmetry is maintained by proteins referred to as flippases and floppases.[1] Morphological changes to lipid membranes due to their asymmetry affect the pharmacokinetics of drug compounds, but current model membranes are not well-suited to modelling membrane asymmetry. For example, loss of bilayer asymmetry is a feature of some types of cancerous cells, with important implications for detection of cancers and their course of treatment.[2,3] The anthracycline class of chemotherapy drugs, including doxorubicin (DOX), are particularly sensitive to these changes in lipid composition.[4] However, it is not possible to model membrane asymmetry using parallel artificial membrane permeation assays (PAMPA)[5] and incorporation of asymmetry in liposomes is more difficult than their symmetric counterparts. Notable techniques for formation of asymmetric liposomes include treating symmetric liposomes with transfer proteins or cyclodextrins,[6,7] manipulation of water-in-oil emulsions,[8] and microfluidic methods,[9] each with their own challenges and caveats.[10] Additionally, computational models have shown that the effect of membrane asymmetry on permeability is highly dependent on curvature.[11] Since liposomes are generally significantly smaller than cells,[12] their correspondingly higher degree of curvature for very small liposomes may provide misleading results. We and others have recently shown that Droplet Interface Bilayers (DIBs) are biomimetic, cell-sized artificial cell models,[13,14] but these simple models can still be developed further to more closely replicate cellular features.

Here we demonstrate for the first time the formation of asymmetric DIBs-based artificial cells using bespoke biomimetic mammalian lipid formulations and show how loss of asymmetry affects DOX permeability. Lipids extracted from natural sources consist of numerous different fatty acid chain lengths and degrees of unsaturation, altering their physical properties and membrane packing characteristics. To date, all asymmetric DIBs have relied on synthetic phospholipids for one or both leaflets and none mimic the asymmetry found in mammalian cells.[14–19] The lipid formulations we use consist of naturally-derived l-α-phosphatidylcholine (PC), l-α-phosphatidylethanolamine (PE), sphingomyelin (SM) and cholesterol (CHOL). See Fig. S1 in the ESI for relevant chemical structures.† We chose to focus on these components of the cell membrane based on prior lipidomics data that quantifies membrane asymmetry.[20] PC and PE are the largest constituents of cell membranes, and are known to display an asymmetric distribu-tion between leaflets, and SM and CHOL are known to coalesce strongly in major structural regions of the cell membrane known as lipid rafts.[21] SM is also nearly exclusively found on the outer

[a] *University of Victoria, Department of Chemistry, Victoria BC, V8W 2Y2, Canada; E-mail: kelvira@uvic.ca*

† Electronic Supplementary Information (ESI) available: materials, lipid formulations, droplet and bilayer size measurements, fluorescence intensity measurements and flux calculations, time lapses of bilayer curvature, interfacial tensions of lipid solutions, curvature of bilayers without SM, original fluorescence images, acknowledgements. See DOI: 00.0000/00000000.

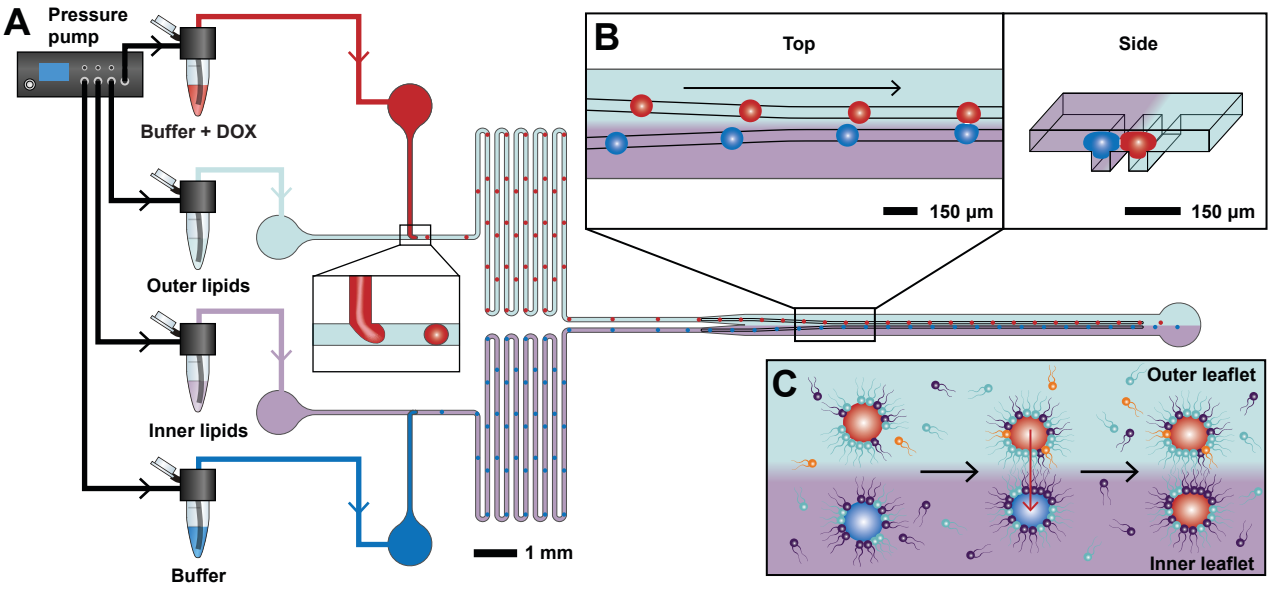

Fig. 1 A) Design of the microfluidic platform showing how the device is connected to the pump and which solution is inserted into each inlet. Aqueous (buffer with DOX, red, or buffer, blue) solutions for the droplets and the surrounding oil phases (different lipid formulations in squalene, light blue and purple) meet at two T-junctions allowing the formation of two different types of droplets surrounded by different lipid monolayers (inset shows red DOX-containing droplet formation). The meanders allow monolayer formation and equilibration before the droplets enter the main chamber. Arrows show direction of fluid flow. The design of the microfluidic device is shown to scale. **B)** Parallel rails are etched into the main chamber of the microfluidic device, bringing the droplets into contact with each other to form DIBs. **C)** Diagram showing the DIB formation process, the localisation of the lipids (not to scale), and subsequent DOX diffusion assays. A DOX-containing aqueous buffer droplet (red) is formed in an oil phase (light blue) containing the lipid formulation that represents the outer leaflet. The interior of this droplet represents the extracellular environment. An aqueous buffer droplet (blue) is formed in an oil phase (purple) containing the lipid formulation that represents inner leaflet. The interior of this droplet represents the interior of the cell. The lipids in the oil phases form a monolayer at the surface of the droplets. The microfluidic device enables the droplets to be brought into contact with each other to form a DIB. DOX then diffuses from the donor droplet to the acceptor droplet (indicated by a red arrow), and the rate of this diffusion is quantified for permeability assays.

leaflet.[20]

We have developed a microfluidic platform that enables the formation of cell-sized asymmetric DIBs using natural lipids dosed in the oil phase (Fig. 1). When forming DIBs, droplets of water are generated in a surrounding oil phase, with phospholipids suspended in either phase. The phospholipids self-assemble at the interface between these two phases in a monolayer, and when the droplets are brought into contact with each other, the mono-layers will zip together to form a bilayer (DIB). Our microfliu-dic device is designed to form two different types of monolayer-covered droplets with a different bespoke lipid formulation dosed in each of the oil phases (Fig. 1A). Full monolayer formation is enabled by adding meanders before gently bringing the droplets together in the main chamber using rails to form DIBs between the droplets (Fig. 1B). Following DIB formation, permeability assays are carried out by observing the diffusion of DOX from the DOX-containing donor droplet to the empty acceptor droplet (Fig. 1C). We demonstrate the formation of stable asymmetric biomimetic DIBs through quantification of bilayer curvature. For asymmetric DIBs, the outer and inner leaflet compositions are shown in Table S2 in the ESI.† To quantify the effect that asymme-try has on DOX permeability, symmetric DIBs were also formed, where a 50:50 mix of the asymmetric lipid formulations were used for both droplets. Partially symmetric DIBs (called "blend") were also formed using a 75:25 mix of the asymmetric lipid formulations for the outer leaflet and a 25:75 mix of the asymmetric lipid formulations for the inner leaflet. Symmetric and blend formulations were prepared immediately before use by combining the required amount of asymmetric inner and outer leaflet solutions. Exact formulations for symmetric and blend DIBs are also shown in Table S2 in the ESI.†

Polydimethylsiloxane (PDMS) microfluidic devices, the aqueous buffer for droplet formation and lipid solutions in squalene (the oil phase for droplet formation) were prepared as described previously,[13] see ESI section 1 for additional details.† Lipid solutions in squalene and aqueous solutions (buffer or buffer with 1 mM DOX) were inserted into the microfluidic device using an Elveflow OB1 mk3 pressure pump at an operating pressure range of 115-145 mbar. Solutions were loaded into Eppendorf tubes and connected to the microfluidic device using matched lengths of 250 μm inner diameter polytetrafluoroethylene (PTFE) tubing (Fig. 1A), and the whole assembly was placed in a custom heat-ing platform[13] on a Nikon Eclipse Ti2-E inverted microscope for visualisation. Experiments were carried out at 50°C, the lowest temperature that allows DIB formation with these naturally derived lipid formulations. Device flow was stopped when a DIB formed and collection of brightfield and fluorescence images was carried out immediately using a Hamamatsu ORCA-Flash4.0 V3 camera and a Solis-1C white LED light source (Thor Labs). Fluorescence images were collected using an mCherry-C filter cube

set (Semrock) with excitation and emission bands of 538-588 nm and 600-685 nm respectively. Images were collected every 5 s for 1 min and then every 20 s for 10 min. These images were collected and then analyzed with NIS Elements Advanced Research (Nikon, 5.11.01). All curvature measurements were carried out at time of 4 min to allow for complete bilayer formation. To normalise droplet curvature measurements for droplet size, the radius of a circle fitted to the inner leaflet droplet on the face opposite the bilayer was measured. Relative curvature was then calculated by dividing droplet radius by the radius of a circle fitted to the bilayer itself. Additional details on these measurements, as well as measurement of fluorescence intensity, droplet size and bilayer size may be found in Fig. S3-5 in the ESI.†

Our microfluidic platform allows the formation of asymmetric DIBs using naturally derived lipids dosed in the oil phase ("lipid-out"). Lipid asymmetry is maintained over at least 10 minutes (see Fig. S6-8 in the ESI†), allowing quantification of the ef-fect that asymmetry has on DOX permeability. Using DIBs formed lipid-in (lipids dosed in the aqueous phase) for pharmacokinetic modelling is difficult, as liposomes present in solution may retain drug and complicate interpretation of drug diffusion. In contrast to most prior work,[15–18] our device uses the lipid-out approach to enable collection of diffusion data. There are two main rea-sons why our device enables the stable formation of asymmetric model membranes. Firstly, squalene is around 13 times more vis-cous than water,[22,23] which means that mixing of the two dif-ferent lipid formulations present in each of the two oil phases is very slow. Secondly, monolayer formation when forming DIBs lipid-out is generally slower than when forming them lipid-in, in large part due to the higher energy barrier to inverse micelle con-tact with the fluid interface of a partially formed monolayer.[24] This suggests that there is also a large energetic barrier to lipid exchange with the oil solutions, leading to a preservation of asymmetry following DIB formation.

Here we show that DIBs can model the curvature of real cells and that this depends on the lipids used. We found that the asymmetric distribution of lipids between leaflets was quantifiable using membrane curvature and that increased bilayer asymmetry leads to an enhanced degree of curvature (Fig. 2). Previ-ous work has shown that asymmetric DIBs made from synthetic phospholipids display curvature based on differing interfacial tension (IFT) of the leaflets.[19] Our natural lipid formulations show an enhanced degree of curvature, more closely replicating the morphology of cellular membranes. The scale of our droplets is similar to that of human cells,[25] and the DIB curvature relative to droplet size approaches 1:1 only for the asymmetric bilayers. Hence, the curvature observed in our asymmetric DIBs mimics the expected curvature for an actual cell, driven by a 20-fold difference in IFT between the leaflets (see Table S9 in the ESI†). This driving force likely differs from those observed in biological membranes, which have considerably lower IFT.[26] Early preliminary experiments showed that the curvature exhibited by membranes consisting of identical concentrations of DOPC, PE and CHOL did not display this dramatic curvature (see Fig. S11 in the ESI†). This suggests that SM contributes the greatest amount to the dif-fering interfacial tension between leaflets. Indeed, this 20-fold

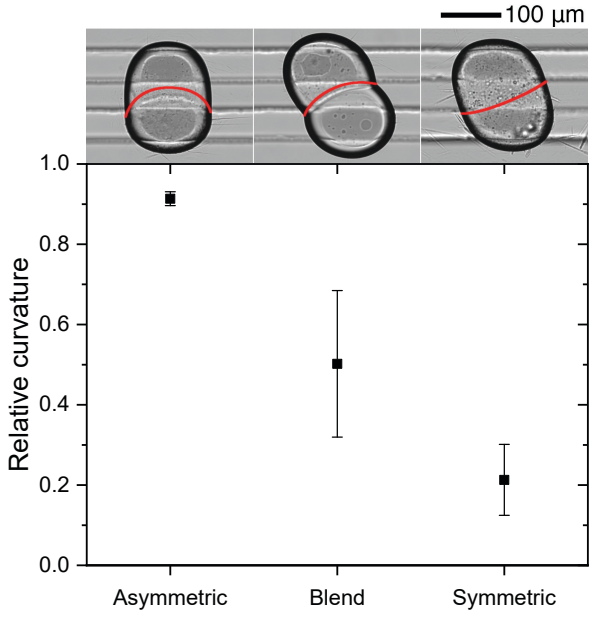

Fig. 2 Relative curvature of asymmetric, symmetric and blend DIBs. Data are normalised for droplet size. Error bars represent the standard deviation (n = 3). Representative images for each formulation are shown above their respective data points, with the measured portion of the bilayer indicated by a red line. The scale applies to all images. The non-spheroidal shape seen in both symmetric bilayer droplets is likely due to the exceptionally low IFT in these bilayers, which also makes them less stable over time.

drop in IFT was observed with addition of only 120 $\mu g\,mL^{-1}$ of SM (see Fig. S10 in the ESI†). The differing curvature conferred by the cylindrical and conical shape of PC and PE respectively appears to be a secondary effect, in agreement with membrane curvature preferences found in the literature.[27]

Our microfluidic platform enables us to create DIBs from bespoke lipid formulations which we can use to distinguish the effect that lipid asymmetry has on DOX permeability. We quantified DOX permeability in asymmetric and symmetric DIBs, and in DIBs made using a blend of asymmetric and symmetric lipid formulations. We found differences in the permeability of our biomimetic model membranes to DOX depending upon their asymmetry and quantified this using fluorescence intensity (Fig. 3). The fluorescence intensity of DOX upon association with phospholipid bilayers is known to be enhanced.[28] This increased intensity of DOX fluorescence is visible in the DIBs as a thin brighter line between the droplets (Fig. 3). This further shows the biomimetic nature of our DIBs since they correctly model the local microenvironment of a cellular membrane, with the visi-ble enhancement of DOX fluorescence serving as evidence of the expected interaction between DOX and the bilayer. We quanti-fied DOX permeability using flux (Fig. 4), which revealed an inverse relationship between membrane symmetry and perme-ability. The cause of this relationship is unclear, but we be-lieve differing IFT and lipid packing are more likely to drive this relationship than the differing curvatures, given that the curved bilayers are effectively planar on the molecular scale. The permeability (P_{app}) for the asymmetric, blend and the symmet-

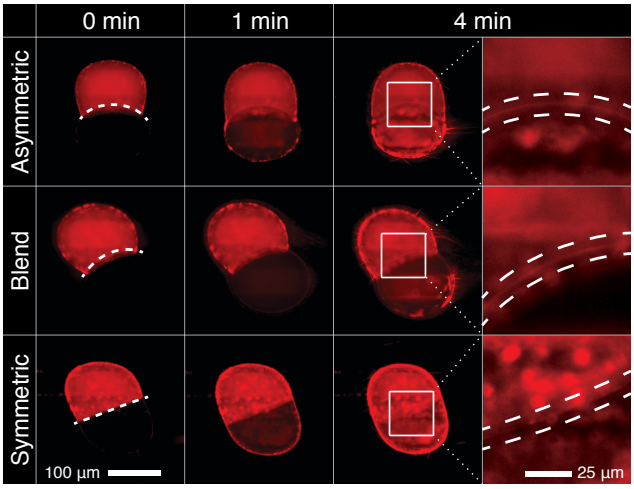

Fig. 3 Diffusion of DOX across asymmetric, blend and symmetric bilayers is shown over time. The initial bilayer location is indicated by a dashed white line for each lipid formulation. The evolution of the bilayer as it forms can be seen, with equilibrium bilayer size and curvature visible at time 4 min. The scale applies to all images in the first three columns. DOX localisation in membrane domains is shown for the last set of images, as indicated by the white squares at time = 4 min. The interaction between DOX and the bilayer is visible in the final column of images as a thin bright line (highlighted with line profiles). This column has been contrast enhanced to aid visualisation. The scale applies to all expanded images. For original images, see Fig. S12-15 in the ESI.†

ric bilayers is $(5.3 \pm 0.2) \times 10^{-6}\,\mathrm{cm\,s^{-1}}$, $(5 \pm 1) \times 10^{-6}\,\mathrm{cm\,s^{-1}}$ and $(4.1 \pm 0.3) \times 10^{-6}\,\mathrm{cm\,s^{-1}}$ respectively. P_{app} in cells can range from $0.3 \times 10^{-6}\,\mathrm{cm\,s^{-1}}$ to $14 \times 10^{-6}\,\mathrm{cm\,s^{-1}}$ depending on cell line and DOX concentration.[29] Our P_{app} therefore is in agreement with data obtained by other *in vitro* methods, although being collected above physiological temperature likely increases measured P_{app}.

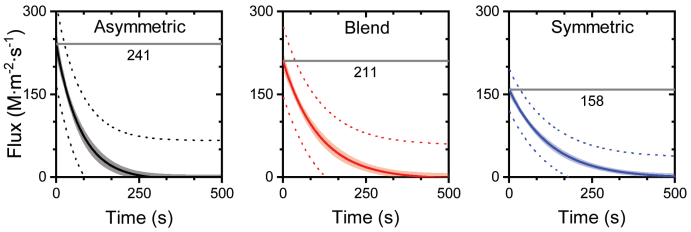

Fig. 4 Flux of DOX over time for asymmetric, blend and symmetric DIBs. Graphs show the trendlines for flux calculated from fluorescence intensity measurements (see ESI section 4 for formulae†) with 95% confidence bands (shaded) and 95% prediction bands (dotted lines) (n = 3). Peak flux is indicated by a horizontal line, with this value used for P_{app} calcula-tions.

In conclusion, our microfluidic platform enables us to build asymmetric bilayers using naturally derived lipids that mimic mammalian cells and use them to quantify the effect that lipid asymmetry has on DOX permeability. Our membrane curvature characterisation revealed that an asymmetric lipid formulation based on the leaflet composition of real cells produces a degree of curvature comparable to that of a biological system. We have hence shown that we are significantly closer to making artificial membranes that are worthy of the title of artificial cell because they truly emulate cell membranes found in nature. By studying the permeability of both symmetric and asymmetric bilayers to DOX, we have found that bilayer asymmetry has a measurable effect on permeability of a membrane to a chemotherapy drug. This not only shines light on one potential mechanism by which tumors may exhibit chemoresistance, but also serves to highlight the importance of fully replicating the structural features of biological systems when studying their pharmacokinetics *in vitro*. The newly demonstrated ability of our biomimetic, asymmetric, DIB-based artificial cells to measure permeability of chemotherapy drugs *in vitro* opens the door to an entirely new kind of pharmacokinetic study for drugs both during and following their development. For acknowledgements and funding sources, see ESI section 9.†

Conflicts of interest

There are no conflicts to declare.

Notes and references

1 H. M. Hankins, R. D. Baldridge, P. Xu and T. R. Graham, *Traffic*, 2015, **16**, 35–47.
2 A. C. Alves, D. Ribeiro, C. Nunes and S. Reis, *BBA - Biomembranes*, 2016, **1858**, 2231–2244.
3 S. Ran and P. E. Thorpe, *International Journal of Radiation Oncology, Biology, Physics*, 2002, **54**, 1479–1484.
4 L. Gallois, M. Fiallo and A. Garnier-Suillerot, *BBA - Biomembranes*, 1998, **1370**, 31–40.
5 M. Kansy, F. Senner and K. Gubernator, *Journal of Medicinal Chemistry*, 1998, **41**, 1007–1010.
6 L. W. Johnson, M. E. Hughes and D. B. Zilversmit, *BBA - Biomembranes*, 1975, **375**, 176–185.
7 H.-T. Cheng, Megha and E. London, *Journal of Biological Chemistry*, 2009, **284**, 6079–6092.
8 S. Pautot, B. J. Frisken and D. A. Weitz, *Proceedings of the National Academy of Sciences*, 2003, **100**, 10718–10721.
9 P. C. Hu, S. Li and N. Malmstadt, *ACS Applied Materials & Interfaces*, 2011, **3**, 1434–1440.
10 M. H. L. Nguyen, B. W. Rickeard, M. DiPasquale and D. Marquardt, *Biomimetic Lipid Membranes: Fundamentals, Applications, and Commercialization*, Springer International Publishing, Switzerland, 2019, pp. 47–71.
11 S. Yesylevskyy, T. Rivel and C. Ramseyer, *Scientific Reports*, 2019, **9**, 17214.
12 T. Rivel, C. Ramseyer and S. Yesylevskyy, *Scientific Reports*, 2019, **9**, 5627.
13 J. L. Korner, E. B. Stephenson and K. S. Elvira, *Lab on a Chip*, 2020, **20**, 1898–1906.
14 S. Bachler, M. Ort, S. D. Krämer and P. S. Dittrich, *Analytical Chemistry*, 2021.
15 W. L. Hwang, M. Chen, B. Cronin, M. A. Holden and H. Bayley, *Journal of the American Chemical Society*, 2008, **130**, 5878–5879.
16 N. E. Barlow, E. Smpokou, M. S. Friddin, R. Macey, I. R. Gould, C. Turnbull, A. J. Flemming, N. J. Brooks, O. Ces and L. M. C. Barter, *Biomicrofluidics*, 2017, **11**, 024107.
17 C. E. Stanley, K. S. Elvira, X. Z. Niu, A. D. Gee, O. Ces, J. B. Edel and A. J. deMello, *Chemical Communications*, 2010, **46**, 1620–1622.
18 G. Taylor, M.-A. Nguyen, S. Koner, E. Freeman, C. P. Collier and S. A. Sarles, *BBA - Biomembranes*, 2019, **1861**, 335–343.
19 N. E. Barlow, H. Kusumaatmaja, A. Salehi-Reyhani, N. Brooks, L. M. C. Barter, A. J. Flemming and O. Ces, *Journal of The Royal Society Interface*, 2018, **15**, 20180610.
20 A. Zachowski, *Biochemical Journal*, 1993, **294**, 1–14.
21 D. Lingwood and K. Simons, *Science*, 2010, **327**, 46–50.
22 J. J. Morgan, W. Stumm and J. D. Hem, *Kirk-Othmer Encyclopedia of Chemical Technology*, American Cancer Society, 2006.
23 M. O'Neil, *The Merck Index - An Encyclopedia of Chemicals, Drugs, and Biologicals*, Royal Society of Chemistry, Cambridge, UK, 2013, p. 1624.
24 G. A. Venkatesan, J. Lee, A. B. Farimani, M. Heiranian, C. P. Collier, N. R. Aluru and S. A. Sarles, *Langmuir*, 2015, **31**, 12883–12893.
25 M. B. Ginzberg, R. Kafri and M. Kirschner, *Science*, 2015, **348**, 1245075.
26 R. David, O. Luu, E. W. Damm, J. W. H. Wen, M. Nagel and R. Winklbauer, *Development*, 2014, **141**, 3672–3682.
27 M. M. Kamal, D. Mills, M. Grzybek and J. Howard, *Proceedings of the National Academy of Sciences*, 2009, **106**, 22245–22250.
28 R. Goldman, T. Facchinetti, D. Bach, A. Raz and M. Shinitzky, *BBA - Biomembranes*, 1978, **512**, 254–269.
29 M. I. Bogorad and P. C. Searson, *Integrative Biology*, 2016, **8**, 976–984.